Analysis and calibration of process variations for an array of temperature sensors

S. Xie[1], A. Abarca[1], J. Markenhof[1], X. Ge[1], A. Theuwissen[1,2]
[1]Electronic Instrumentation Laboratory, TU Delft, Delft, The Netherlands
[2]Harvest Imaging, Bree, Belgium
s.xie@tudelft.nl

***Abstract*—This paper presents an analysis and calibration of process variations for an array of temperature sensors, which are incorporated into a CMOS image sensor chip. Making use of the experimental results of more than 500 temperature sensors implemented on the same chip, the proposed calibration method has removed their process variations from 14.3 % to 2.5 % (3 sigma).**

Keywords—BJT based temperature sensor; CMOS image sensor; sensor array; calibration

I. INTRODUCTION

Over 500 temperature sensors are incorporated into a 4T Pinned Photodiode (PPD) CMOS image sensor (CIS) array for dark current prediction. In CIS, dark current stands for the signal response when a photo detector is not exposed to light. It not only limits the full-well capacity but also creates dark fixed pattern noise (FPN) and dark current shot noise in CIS. Despite its complex generation process, dark current in the majority of pixels in a 4T PPD CIS is proportional to intrinsic carrier concentration n_i^2 [1], which doubles for every 5 ºC of temperature rise. This direct proportional relationship between the dark current and the temperature makes it possible to predict the dark current based on temperature measurements. The target applications are low cost CISs, where no physical shutter is available for capturing dark images. With the aid of temperature sensors, a dark image taken beforehand (e.g., in the factory) at room temperature can be used to predict the dark current for the operating temperatures (e.g., any temperature between -40 ºC and 90 ºC).

The accuracy required for temperature sensors aimed for dark current prediction is 1 ºC [2]. In our test device, each temperature sensor occupies the area of two image pixels. Although the BJT based temperature sensors are known for relatively less process variations (without calibration, compared to their counterparts [3]), their biasing and amplifying circuits have made the process variations non-trivial, due to the latter's limited circuit area and larger spatial distances apart. On one hand, a two-point or best-curve fitting [4] is always feasible in the laboratory to calibrate each of the over 500 sensors, thus removing their process variations; on the other, a one-point alternative is more time efficient and can be performed at the same time when taking the dark image at room temperature, as mentioned in the previous paragraph. In other words, a one-point calibration method is more suitable for mass production.

The authors acknowledge the support of TowerJazz in realizing the prototype CIS devices. The research is part of the CISTERN project, funded by the Dutch government through the CATRENE initiative.

The rest of this paper is organized as follows. Section II gives an analysis of the sources of process variations. Section III proposes the calibration method. In Section IV, the experimental results with and without using the proposed calibration method are reported. This is followed by conclusions in Section V.

II. SOURCES OF PROCESS VARIATIONS

A. Process variations among the temperature pixels

The analysis begins with the operating principle of the temperature sensor, or the temperature pixel (Tixel), as shown in Fig. 1 (a). When *CS (j)* and *RS (i)* are both on, the Tixel is selected and *Q1*, which is a substrate bipolar junction transistor (BJT), has its emitter-base voltage (*VEB*) proportional to the current *Ibias* going into its emitter. Having two different *Ibias* levels, e.g., *Ibias1* and *Ibias2*, going into its emitter sequentially, the change in *Q1*'s *VEB* (*ΔVEB*) can be expressed as [4]:

$$\Delta VEB = \frac{kT}{q} ln(N) \quad (1)$$

Where

$$N = Ibias1/Ibias2 \quad (2)$$

Where k is the Boltzmann constant and T is the temperature, while q is the elementary electron charge. From the voltage level of *ΔVEB*, the temperature can be deduced. *ΔVEB* has been demonstrated to be less sensitive to process variations than *VEB* itself [4]. The only parameter in (1) that depends on process or mismatches is *N*—the ratio of the two biasing currents, which are generated using the row level circuit illustrated in Fig. 1 (b). During the first phase, all S<0>~<3> are on, generating a current *Ibias1* that is 4 times as large as *Isource* (assuming the pMOS current mirror's ratio is 1:1); during the second phase, only one switch, e.g., S<0> is on, so *Ibias2* is as the same level as *Isource*. Monte Carlo mismatch simulation shows that the current ratio mismatch with and without dynamic element matching (DEM) are ±0.249 % and ±0.251 % (3 sigma), respectively, for pMOS current mirror transistor, each area of 8 µm×8 µm. This translates to process variations of around ±0.25 ºC in temperature, when using a best curve fitting for a 100 ºC temperature range.

On the other hand, non-ideal factors which are invisible in (1), such as series resistances, reverse Early effect, and saturation currents [4], have given rise to process variations

978-1-5090-1012-7/17/$31.00 ©2017 IEEE

among *ΔVEB*, even under ideal current biasing conditions, as demonstrated in the simulation results plotted in Fig. 2. The deviations from SS or FF to TT corner (shown in Fig. 2) are around ±1 %, which equals approximately 1 °C in temperature.

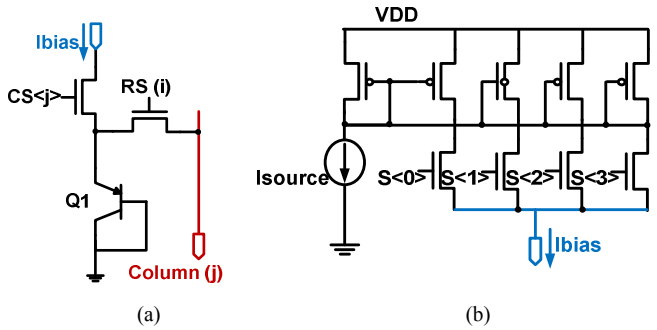

(a) (b)

Fig. 1. Schematic of (a) the temperature pixel (Tixel) and (b) the current mirror circuit for biasing the temperature pixel shown in (a).

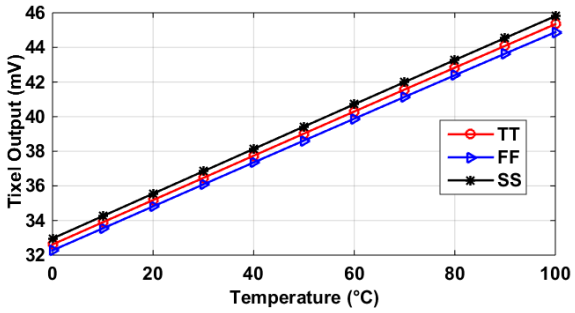

Fig. 2. Simulation results of *ΔVEB*, for corners TT, FF and SS in Cadence Virtuoso. All current sources and other transistors are simulated using ideal components without any mismatch except for the BJT *Q1* shown in Fig. 1 (a).

B. Process variations among the column circuits

The temperature pixel shown in Fig. 1 (a) is read out through the column bus (labeled as "column (j)"), which is connected to *Vin* (the input of a programmable amplifier (PGA)) drawn in Fig. 3. This PGA is intended for the image sensors on the same chip, to accommodate for lower noise with higher PGA gain and wider dynamic range with lower PGA gain. The Tixels make use of the same column PGAs for minimum hardware complexity. During the first phase, the switch *RST* is closed, and the output *VPGA* equals *Vref* plus the offset voltage of the amplifier *Ao*. During the second phase, the switch *RS* is open and the difference between *Vin* voltages of the two phases is approximately amplified to be:

$$\Delta VPGA = \Delta Vin \cdot \frac{C1}{C2} \tag{3}$$

ΔVin and ΔVPGA stand for the changes in *Vin* and *VPGA* between the two phases, respectively. As *ΔVin = ΔVEB* for temperature sensors, by taking (1) into (3):

$$\Delta VPGA = T\frac{k}{q}\frac{C1}{C2}ln(N) \tag{4}$$

ΔVPGA is therefore an amplified voltage of *ΔVEB,* which is proportional to temperature. Due to the closed loop feature of the PGA, the majority of the mismatches in (3) come from those between the capacitors C1 and C2. The mismatches obtained from the technology datasheet are 0.2 % for typical case, and are simulated to be around ±0.46 % (3 sigma) in Cadence Virtuoso, as shown in Fig. 4. The latter mismatches translate to ±0.46 °C in temperature measurements.

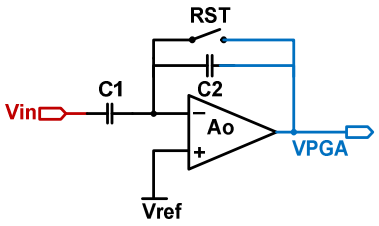

Fig. 3. The schematic of the column PGA circuit [5].

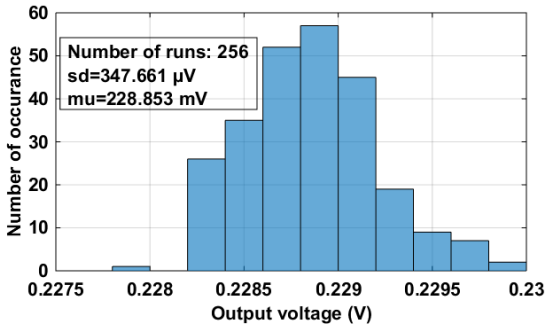

Fig. 4. Monte Carlo simulation results of the PGA output voltage. The input voltage *ΔVin* is 30 mV and the PGA nominal gain is 8. In the graph, "mu" is the averaged output voltage, and "sd" is the 1 sigma variation voltage.

III. CALIBRATION METHODS

Observing (3), one may conclude that except for the temperature *T*, all other factors are either constants or only related to process variations. Therefore, *ΔVPGA* can be expressed as the product of a temperature-dependent part *T* and a temperature-independent part *G(P)*[6]:

$$\Delta VPGA(T,i,j) = T \cdot G(P) \tag{5}$$

Where *ΔVPGA(T,i,j)* refers to the PGA output of the temperature pixel located at the i-th row and the j-th column in the array and while *T* is the measured temperature and $G(P) = \frac{k}{q}\frac{C1}{C2}\ln(N)$ in this work. Instead of adjusting the temperature sensor output voltage to be the same at room temperature as proposed in [6], a correction factor N_C for each sensor can be computed and assigned [7]:

$$N_C(i,j) = \frac{CT_C}{\Delta VPGA(Tc,i,j)} \tag{6}$$

$N_C(i,j)$ is the correction factor for the temperature sensor located at the *i*-th row and the *j*-th column in the array while T_C is the calibration temperature (e.g., room temperature). CT_C is an arbitrary constant number assigned by the designer and this number is the same for all the temperature pixels. Then, by multiplying this correction factor $N_C(i,j)$ with the output *ΔVPGA(T,i,j)* of the same temperature pixel from which it is computed, at any other operating temperature *T*, the calibrated output becomes:

$$C(T,i,j) = N_C(i,j) \cdot \Delta VPGA(T,i,j)$$
$$= \frac{CT_C}{\Delta VPGA(Tc,i,j)} \cdot \Delta VPGA(T,i,j) = CT_C \cdot \frac{T}{T_C} \tag{7}$$

Eventually, the calibrated output $C(T,i,j)$ is only with the constant CT_C, the calibration temperature T_C and the measured temperature T. It is only proportional to temperature, without being sensitive to process variations.

IV. Experimental Results

A prototype for incorporating 555 temperature sensors into a CIS chip has been fabricated in 0.18 µm CIS technology. The temperature sensors are distributed in a semi-uniform pattern and are measured in a temperature chamber from 30 ºC to 70 ºC at every 10 ºC. Their analog outputs from the chip are quantized by an on-board ADC (AD9826) and read out by LabVIEW into an Excel file, which is further processed in MATLAB, using the calibration method proposed in Section III. The accuracy of the measured temperature is determined by the ADC, to be 0.025 ºC. The calibration method proposed in (7) is performed in the digital domain, using the ADC's outputs, which are digital representations of the chip's analog output $\Delta VPGA$ shown from (3) to (7). Fig. 5 shows the measured temperatures and errors from 555 temperature sensors, using i) a global best curve fitting for the averaged output of all the sensors (red line); ii) a global best curve fitting for all the sensors (blue lines); iii) a best curve fitting for each individual sensor (green lines); iv) a one-point calibration for each sensor at the same time, as proposed in section III, followed by a global best curve fitting for all the sensors (pink lines). Fig. 5 (b) shows that compared to the case without calibration, the process variations are reduced from ±14.3 ºC (blue lines) to ±2.5 ºC (pink lines). The 3 sigma errors when using best curve fitting for each sensor is ±1.8 ºC. The curvature of i) averaged output is 0.2 ºC, so one may conclude that the majority of the errors plotted in Fig. 5 originating from using methods ii) and iii) are process variations. The errors not removed by the calibration method iv) can be due to the non-idealities not shown in (1): e.g., the saturation current is in fact a part of (2)'s denominator and nominator, and it varies with process parameters such as doping and geometry. The 3 sigma process variations using ii) a global best curve fitting is much larger than the values simulated in Section II. This could be explained by power supply level variations across the entire chip. Furthermore, due to systematic offsets, the doping and physical variations could be more than those simulated.

V. Conclusions

A calibration method for removing process variations among multiple BJT based temperature sensors has been proposed. It reduces the process variations among the 555 sensors implemented on the same CIS chip, from ±14.3 % to ±2.5 % (3 sigma), using experimental results. The proposed calibration can be performed at the same time when capturing the dark image for dark current compensation, at room temperature, so its required calibration effort is negligible, compared to an alternative using a best curve fitting for each sensor.

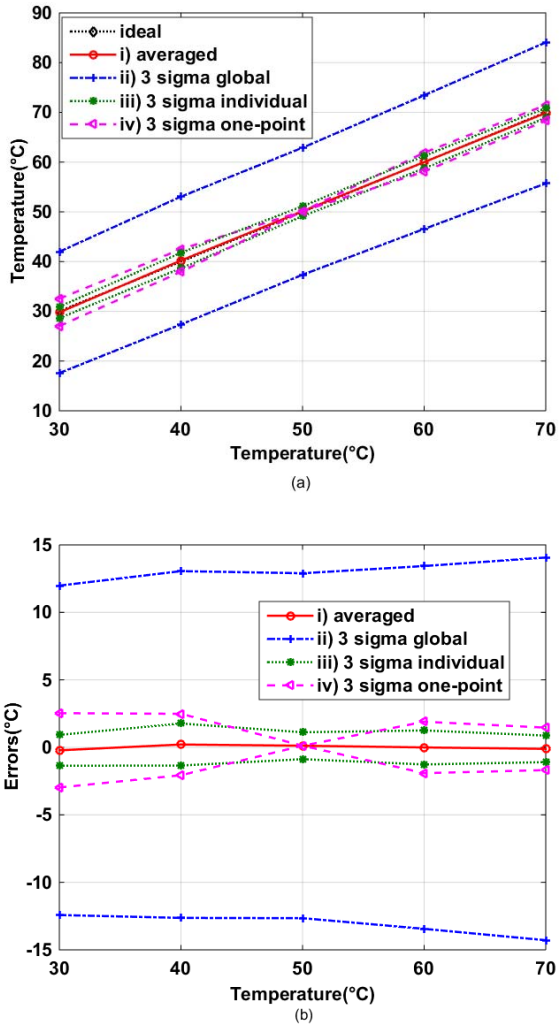

Fig. 5. Measured (a) temperatures and (b) errors from: i) the averaged output from all the 555 sensors (red line); ii) using a global best curve fitting of the averaged output for all the sensors (blue lines for 3 sigma outlines); iii) best curve fitting for each sensor (green lines for 3 sigma outlines); and iv) calibration at one-point (50 ºC) for each sensor at the same time, using the method proposed in Section III, followed by a global best curve fitting for all the sensors (pink lines for 3 sigma outlines).

References

[1] X. Wang. Noise in Sub-Micron CMOS Image Sensors. PhD Dissertation, TU Delft, the Netherlands. 2008, pp. 46–68.

[2] A. Theuwissen, "How to measure the average dark signal", available online at: http://harvestimaging.com/blog/?p=795.

[3] K.A.A. Makinwa, TU Delft, "Smart Temperature Sensor Survey," available online at: ei.ewi.tudelft.nl/docs/TSensor_survey.xls, Feb 2017.

[4] M.A.P. Pertijs and J.H. Huising. Precision Temperature Sensors in CMOS Technology. Springer. 2006, pp. 11–102.

[5] X.Ge.The Design of a Global Shutter CMOS Image Sensor in 110nm Technology. Master Thesis, TU Delft, Netherlands, 2012, pp. 73–74.

[6] D. Ha, K. Woo, S. Meninger, T. Xanthopoulos, E. Crain, and D. Ham,"Time-Domain CMOS temperature sensors with dual delay-locked loops for microprocessor thermal monitoring," in Trans.VLSI, vol.20, no.9, pp.1590–1601, Sep. 2012.

[7] S.Xie and W.T. Ng, "A low power all-digital self-calibrated temperature sensor using 65nm FPGAs", in Proc. ISCAS, May 2013, pp. 2617–2620.